ACS APPLIED MATERIALS & INTERFACES

Research Article

www.acsami.org

Advanced Phase Change Composite by Thermally Annealed Defect-Free Graphene for Thermal Energy Storage

Guoqing Xin,[†] Hongtao Sun,[†] Spencer Michael Scott,[†] Tiankai Yao,[†] Fengyuan Lu,[†] Dali Shao,[‡] Tao Hu,[†] Gongkai Wang,[†] Guang Ran,[§,*] and Jie Lian[†,*]

[†]Department of Mechanical, Aerospace and Nuclear Engineering and [‡]Department of Electrical, Computer & Systems Engineering, Rensselaer Polytechnic Institute, 110 Eighth Street, Troy, New York 12180, United States

[§]College of Energy, Xiamen University, Xiamen, Fujian 361005, China

Supporting Information

ABSTRACT: Organic phase change materials (PCMs) have been utilized as latent heat energy storage and release media for effective thermal management. A major challenge exists for organic PCMs in which their low thermal conductivity leads to a slow transient temperature response and reduced heat transfer efficiency. In this work, 2D thermally annealed defect-free graphene sheets (GSs) can be obtained upon high temperature annealing in removing defects and oxygen functional groups. As a result of greatly reduced phonon scattering centers for thermal transport, the incorporation of ultralight weight and defect free graphene applied as nanoscale additives into a phase change composite (PCC) drastically improve thermal conductivity and meanwhile minimize the reduction of heat of fusion. A high thermal conductivity of the defect-free graphene-PCC can be achieved up to 3.55 W/(m K) at a 10 wt % graphene loading. This represents an enhancement of over 600% as compared to pristine graphene-PCC without annealing at a comparable loading, and a 16-fold enhancement than the pure PCM (1-octadecanol). The defect-free graphene-PCC displays rapid temperature response and superior heat transfer capability as compared to the pristine graphene-PCC or pure PCM, enabling transformational thermal energy storage and management.

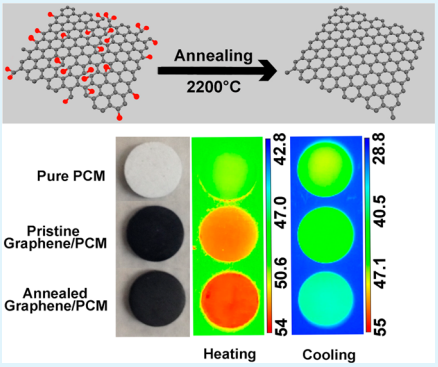

KEYWORDS: *phase change materials, graphene, thermal energy storage, thermal conductivity, phase change enthalpy*

1. INTRODUCTION

Organic phase change materials (PCMs) have drawn significant attention because of their ability to store and release thermal energy with high storage capacity (heat of fusion at the order of 200 J/g) cycling through liquidation and solidification within a small temperature range.[1−5] In addition to the high energy storage capacity, the high chemical and thermal stability, no subcooling required, and no corrosivity make organic PCMs promising for latent heat storage and transfer in applications of effective thermal management of electronic devices, thermal energy storage, and even as a heat transfer media.[1−3] However, a major drawback of organic PCMs is their low thermal conductivity, leading to a slow response to temperature change and reduced heat transfer efficiency.[1−3] Conventional efforts to develop advanced PCMs focus primarily on improving the thermal transfer efficiency using mechanically supporting and thermally conductive foams or compressed graphite matrices,[6−10] or synthesis of phase change composites (PCCs) by mixing the PCMs with thermally conductive fillers of various materials and shapes such as graphite nanoplatelets, expanded graphite, carbon nanotubes and nanofibers, and dispersing PCMs into highly thermally conductive porous structures.[11−25] However, the use of such solid matrices or the incorporation of additives that do not undergo a phase change, displace a significant portion of the PCM volume, reducing the heat storage capability.[7,11,12,14,18,20−22,26] Inefficiencies in heat transfer also occur across interfaces between adjacent nanofills and PCM matrix. It is still a challenge in developing advanced PCMs to achieve simultaneously enhanced thermal transfer and energy storage capability.

Graphene, a single layer of graphite, has an ideal two-dimensional structure of carbon hexagons.[27−30] The strong and anisotropic sp^2 bonding and the low mass of the carbon atoms give graphene unique thermal properties.[27,29,30] The in-plane thermal conductivity of graphene at room temperature is among the highest of any known materials, about 2000−4000 W/(m K) for freely suspended samples, an order of magnitude higher than that of copper.[27,29,30] The ultrahigh thermal conductivity makes graphene promising for thermal management, behaving as thermally conductive fillers in polymer composites and graphene paper in heat spreaders.[27,29,30] Large scale graphene nanosheets are typically produced by solution approaches, e.g., the reduction of graphene oxides or direct exfoliation of graphite for practical applications.[28,31−33]

Received: June 8, 2014
Accepted: August 11, 2014
Published: August 11, 2014

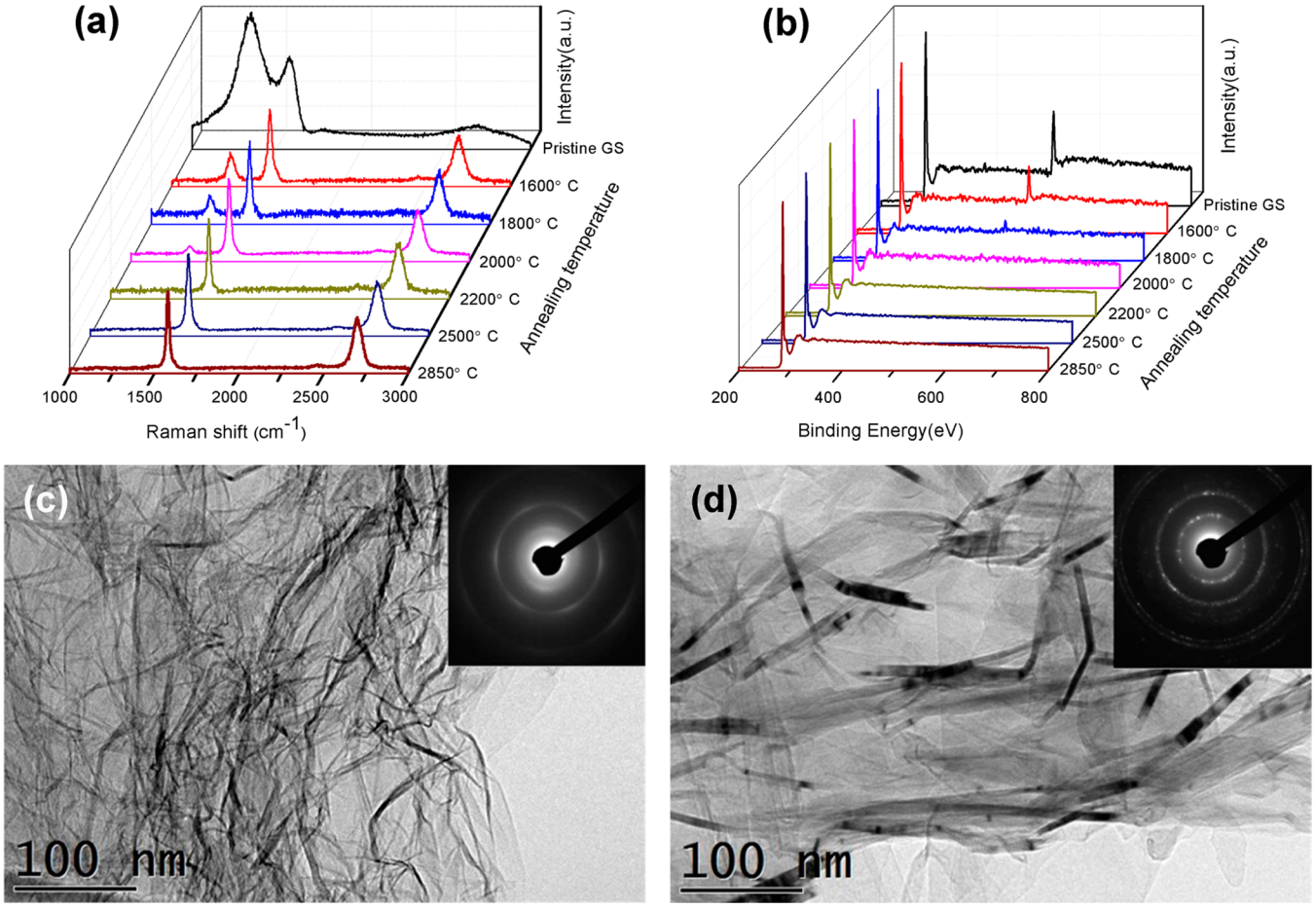

Figure 1. Defect-free graphene sheets by high-temperature annealing: (a) Raman spectra of pristine and annealed GSs; (b) XPS spectra of pristine and annealed GSs; (c, d) TEM image of (c) pristine graphene and (d) GSs annealed at 2200 °C. Insets in c and d show selected area electron diffraction (SAED) patterns of the GSs.

However, the exceptional thermal properties of high-quality graphene cannot be realized from GSs prepared by chemical approaches. The residual functional groups and defects existing on GSs from chemical processes is inevitable,[14,28,31−36] leading to significant degradation of its thermal properties.[27,29,30] Chemically or thermally reduced GSs and exfoliated GSs have been used to improve thermal conductivity of different organic materials such as epoxy, poly(vinyl alcohol), and poly(vinylidene fluoride).[37−39] However, a large amount of low-quality defect GS is required because of its inferior thermal properties, and thus further degrading the mechanical properties and latent of heat of the composite.[37−39]

Previously, high-temperature thermal annealing was proposed as an effective approach to remove defect and produce high-quality GSs with greatly improved electron mobility; however, residual oxygen groups and defects still exist from high-temperature annealed GSs.[40−42] In this work, thermal treatment was optimized, enabling high-quality GSs free of defects and oxygen functional groups. The elimination of defects and oxygen functional groups on GSs reduces effective phonon scattering centers and improve their thermal properties.[27,29,30] The ultrahigh thermal conductivity and ultralight weight make defect-free GSs ideally as thermally conductive fillers for PCMs. We fabricate PCM composite with well-dispersed defect-free GSs displaying a drastically improved thermal conductivity and minimized reduction of the heat of fusion. The defect-free graphene PCM composite displays an over 600% improvement in thermal conductivity as compared with defective graphene composite and meanwhile maintain the latent of heat at the order of 200 J/g. Rapid temperature response and superior heat transfer capability are also demonstrated for the defect-free graphene/PCMs as compared with composites using defective graphene sheets, graphite nanoplatelets, carbon nanotubes/nanofibers as nanoscale-fillers previously reported.[13−15,20,21] Building up a superfast thermal transport pathway with ultralight and highly thermally conductive graphene as nanofillers at a low volume fraction may enable transformational performance in addressing the key technological challenge to develop advanced PCMs with simultaneously enhanced thermal transfer and energy-storage capabilities.

2. EXPERIMENTAL SECTION

Graphene Synthesis. GSs were fabricated by thermal exfoliation and reduction of the graphite oxide (GO) prepared from graphite power following the Hummers' method, as described elsewhere.[14,31,32] Graphite powder (5 g) was added to a mixture containing concentrated H_2SO_4 (115 mL) and $NaNO_3$ (2.5 g) in an ice bath (0 °C). $KMnO_4$ (15 g) was then added carefully to the solution and maintained for 30 min at 35 °C followed by the slow addition of DI water (230 mL). The temperature of the reaction was maintained at 98 °C for 15 min. After that, additional deionized water (355 mL) containing H_2O_2 (3 wt %, 5 mL) was added. The solid obtained from centrifugation (3200 rpm, 5 min) was washed with excess deionized water, 20 vol % HCl, and ethanol. The washing process was repeated

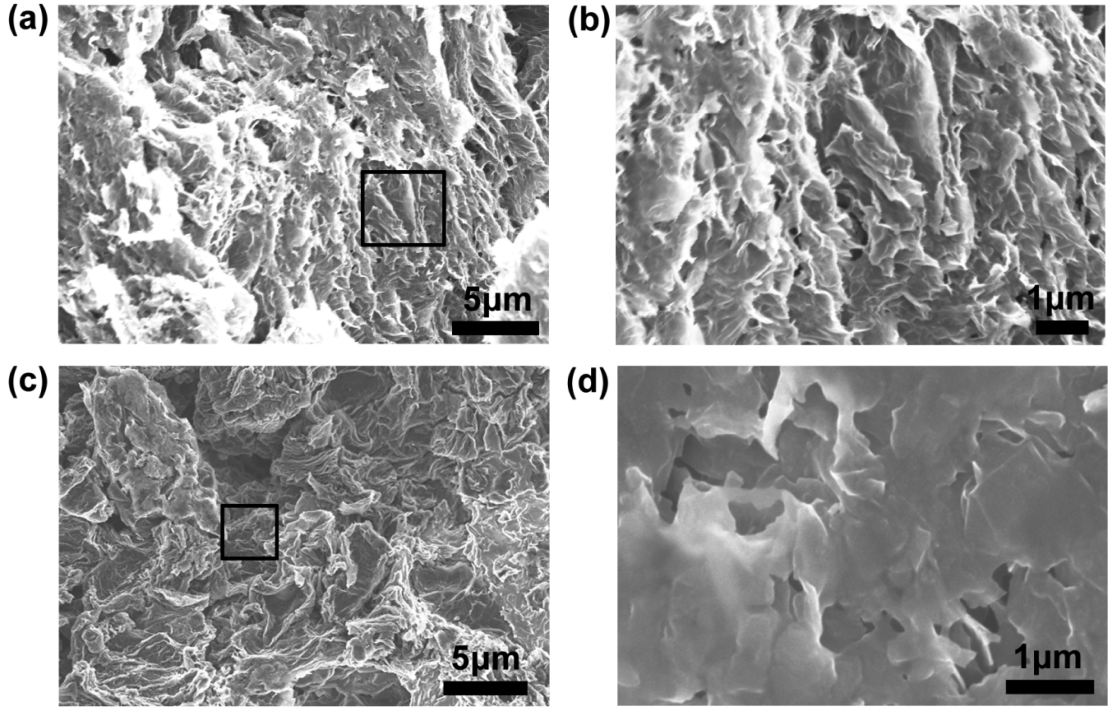

Figure 2. SEM images showing morphology of graphene-phase change composites at a graphene loading of 10 wt %: (a) pristine graphene/PCC (PGPCC) at low magnification; (b) a close-up image from the square in a; (c) annealed graphene/PCC (AGPCC) at low magnification; and (d) a close-up image from the square in c.

several times until the pH of the solution reached neutral. The final yellow brown GO powders were dried under a vacuum at 40 °C for 12 h.

Thermal exfoliation of GO was achieved by placing the GO powder (200 mg) in a 20 mm inner-diameter, 1 m long quartz tube that was sealed at one end. The other end of the quartz tube was closed using a rubber stopper. An argon inlet was then inserted through the rubber stopper. The sample was flushed with argon for 10 min, and the quartz tube was quickly inserted into a tube furnace (Thermolyne 79300, Thermo Fisher Scientific Inc., USA) preheated to 1050 °C and held in the furnace for 30 s. Rapid heating (>2000 °C/min) splits the GO into bulk quantities of few-layered GSs. The mechanism of exfoliation is mainly the production and expansion of H_2O and CO_2 evolved between the graphene sheets during rapid heating. The pressure generated from evolved gases that cause rapid expansion exceeds the van der Waals forces holding GO sheets together to get a successful exfoliation.

Annealing GS at High Temperature. GSs obtained from thermal exfoliation were annealed by using an electrical furnace. Typically, thermal exfoliated GS (1 g) was put in a graphite crucible with lid covered and heated up from room temperature to various temperatures (1600, 1800, 2000, 2200, 2500, and 2850 °C) at a rate of 1000 °C/h and kept at this temperature for 30 min in a flow of argon.

PCC Synthesis. 1-octadecanol was chosen as matrix for the PCCs. First, the 1-octadecanol was melted on hot plate at 120 °C and methanol was added to dissolve 1-octadecanol. Separately, pristine GSs and GSs annealed at 2200 °C were dispersed in the methanol with a tip (bar type) sonication instrument at 400 W for 15 min. The 1-octadecanol solution was then mixed with the graphene dispersions and was sonicated for another ∼15 min. The mixture of graphene and 1-octadecanol in methanol were stirred and heated to ∼150 °C to evaporate the remaining methanol. The nanocomposite in liquid phase was then poured into preheated stainless steel molds of cylindrical shape, 1−2 mm thick and ∼12.70 mm in diameter, and was left at room temperature to solidify for ∼20 min. The resulting composite was affixed to a sample holder, cut to different thicknesses, and polished on a sand paper pad.

Characterization. Thermal conductivity measurements were conducted with a Netzsch LFA 447 NanoFlash instrument. TEM was performed on a JEOL 2010 with a 200 keV accelerated electron beam. Carbon-coated or holey carbon coated copper grids were used in the imaging experiments. The morphology and microstructure of materials were determined by a field-emission SEM on a JEOL (JSM-6335). X-ray photoelectron spectroscopy (XPS) was carried out on a PHI 5000 Versa Probe system. Raman study of GPs was performed with a LabRAM HR800 Raman microscope using a 532.18 nm green laser as the probing light source and 600 g mm^{-1} grating. The scattered light was collected in the backscattering geometry using a CCD detector. A FLIR A325sc infrared camera was used to record the heat transfer on PCM composite disks. The phase change enthalpy of graphene-PCM composite was measured via differential scanning calorimeter (DSC, TA Instruments Q100). The surface area was measured using a Micromeritics ASAP2000 instrument.

3. RESULTS AND DISCUSSION

3.1. Defect-Free GS Preparation. Thermal exfoliation of graphene oxides prepared by solution approaches is an effective process for large-scale synthesis of GSs.[26,28,31−33] In this work, pristine defective graphene nanosheets were prepared by thermal exfoliation with an extremely large surface area up to 1200 m^2/g as confirmed by the Brunauer−Emmett−Teller (BET) measurements. Therefore, significant lattice defects and oxygen functional groups induced by thermal reduction of the graphene oxides exist, as evidenced by the intense D-band at near 1350 cm^{-1} relative to the G band in the Raman spectra (Figure 1a).[40−42] High temperature thermal annealing at various ascending temperatures in vacuum can gradually remove defects and recover crystallinity of the GSs with increasing annealing temperatures.[40−42] The defect removal can be evidenced by the intensity reduction of the D band, narrowing of the G band, and recovery of the 2 D band intensity in the Raman spectra. The defect and oxygen-free and highly crystalline GSs can be achieved at an optimized

temperature of 2200 °C, and further increasing in annealing temperature will not improve the quality of graphene sheets. For example, at optimized thermal treatment at 2200 °C or above, defects are completely removed and no D bands can be identified (Figure 1a).[40−42] XPS spectra indicate the removal of oxygen functional groups from the GSs upon thermal annealing, since the O 1s peak intensity decreases gradually with increasing annealing temperature (Figure 1b).[40−42] The removal of oxygen functional groups can also be observed from the deconvoluted C 1s XPS spectra from pristine GSs and annealed GSs (Figure S1). The oxygen species of C−O (hydroxyl and epoxy) and C═O (carbonyl) groups were reduced continuously with ascending annealing temperatures. When annealed above 2000 °C, the oxygen functional groups have been completely removed, as evidenced by the vanishing of the O 1s peak as compared with the pristine GSs (Figure 1b) and the only remaining C═C peak on the deconvoluted C 1s XPS spectra (Figure S1).[40−42] Bright-field TEM images and selected area electron diffraction (SAED) (inset in Figures 1c and 1d) further prove the recovery of crystallinity of graphitic structure for the defect-free graphene sheet upon high temperature annealing.[28,33] A high degree of graphitization of GSs is achieved during annealing, as evidenced by the discrete diffraction spots in the SAED ring patterns.[28,33] Systematic structural characterizations of the GSs upon thermal treatment demonstrate that 2200 °C is the optimized temperature for achieving defect-free and high-quality graphene with superior properties. As a result, GSs annealed at 2200 °C are applied as thermal conductive fillers to improve the thermal conductivity of PCC composites.

3.2. Highly Thermal Conductive PCCs. 1-Octadecanol (stearyl alcohol), a widely used organic PCM with a low melting temperature of ∼66 °C and an outstanding solid−liquid phase change enthalpy (∼250 J/g), was selected as the model system for proof-of-concept demonstration of the defect-free graphene phase change composite. To improve the thermal conductivity of PCM, a continuous network of well-dispersed conductive filler is essential, allowing phonons to travel efficiently inside of PCM through the conductive fillers. In this work, 1-octadecanol was first melted and dissolved in methanol, and pristine GSs and 2200 °C annealed GSs were well dispersed in methanol with different fraction and then mixed with the 1-octadecanol/methanol solution under ultrasonication. After evaporation of the solvent, the PCCs with a uniform distribution of GSs can be achieved. SEM images (Figures 2a and 2c) show the morphology and dispersion of the freeze-fractured surfaces of annealed graphene/PCC (AGPCC) and pristine graphene/PCC (PGPCC) at a loading of 10 wt % graphene. High-magnification SEM images of the composites are also shown in images b and d in Figure 2, respectively. GSs are covered with a thick layer of 1-octadecanol, without any segregation found between the GSs and matrix. GSs are uniformly dispersed throughout the matrix because of the compatible interface between the GSs and 1-octadecanol, enabling a three-dimensional network of superfast heat conduction.

Thermal conductivity of the fabricated graphene/PCM composites is measured by a "laser flash" technique, and pure 1-octadecanol as a control sample was also measured to benchmark the improvement of the thermal properties of the composites. The measured thermal conductivity for the pure PCM, K = 0.22 W/(m K) at room temperature, is in agreement with the value reported in a previous literature.[43] The efficiency in using highly conductive filler in the graphene-PCCs is characterized by the thermal conductivity enhancement factor (TCE), defined as $\eta = (K_c - K_m)/K_m$, where K_c and K_m are thermal conductivity of the composite and the pure matrix, respectively. Panels a and b in Figure 3 show thermal

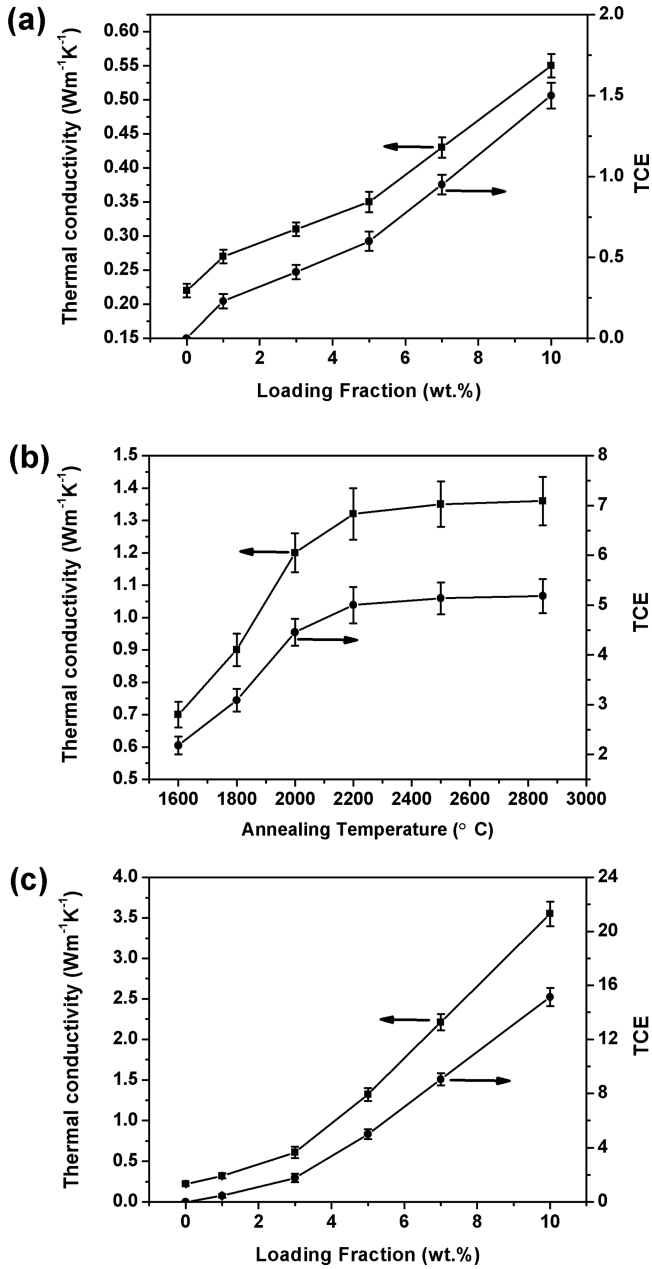

Figure 3. Thermal conductivity and thermal conductivity enhancement factor of graphene-PCCs: (a) pristine graphene/PCC (PGPCC) at various mass loading fraction of GSs; (b) annealed graphene/PCC (AGPCC) at 5 wt % loading fraction of GSs with various annealing temperatures; and (c) annealed graphene/PCC (AGPCC) at various mass loading fraction of GSs annealed at 2200 °C.

conductivity and TCE as a function of loading faction of GSs for both pristine graphene/PCC and defect-free graphene/PCC at room temperature, respectively. Thermal conductivity is considerably enhanced by the presence of GSs. As the loading of pristine GSs varying from 1 to 10 wt %, the thermal conductivity of the pristine graphene/PCC doubles from 0.27

Table 1. Thermal Conductivity Enhancement in PCM Composites

filler	matrix	fraction (wt %)	K (K_m) (W/(m K))	TCE	ΔH (J/g)	measurement method	ref
pristine GS	1-octadecanol	10	0.55 (0.22)	1.5	199	laser flash	this work
annealed GS	1-octadecanol	5	1.32 (0.22)	5	221	laser flash	this work
annealed GS	1-octadecanol	7	2.21 (0.22)	9.0	210	laser flash	this work
annealed GS	1-octadecanol	10	3.55 (0.22)	15.1	195	laser flash	this work
graphene	1-octadecanol	4	0.91 (0.38)	1.39	210	steady-state method	ref 26
graphene	paraffin	10	0.5 (0.25)	1		hot disc thermal constant analyzer	ref 20
graphene nanoplatelets	paraffin	5	0.7 (0.263)	1.66	186	transient hot-wire method	ref 14
sulfonated graphene	polyethylene glycol	4	1.042 (0.263)	2.96	166	laser flash	ref 11
graphene aerogel	octadecanoic acid	15	2.635 (0.184)	13.3	181.8	laser flash	ref 12
graphite nanoplatelets	paraffin	5	0.75 (0.26)	1.88	158.9	astm e1530	ref 18
graphite nanoplatelets	paraffin	10	2.7 (0.25)	9.8	/	hot disc thermal constant analyzer	ref 20
expanded graphite	paraffin	10	0.82(0.22)	2.73	178.3	transient hot-wire method	ref 10
carbon nanofiber	paraffin	5	0.305(0.263)	0.29	185	transient hot-wire method	ref 14
carbon nanofiber	soy wax	10	0.469(0.324)	0.45	/	transient hot-wire method	ref 17
carbon nanofiber	paraffin	10	0.45(0.32)	0.41	/	transient hot-wire method	ref 17
carbon nanotube	palmitic acid	5	0.402(0.318)	0.26	173	hot disc thermal constant analyzer	ref 13
carbon nanotube	soy wax	10	0.403(0.324)	0.24	/	transient hot-wire method	ref 17
short-carbon nanotube	paraffin	5	0.324 (0.263)	0.23	178	transient hot-wire method	ref 14
long- carbon nanotube	paraffin	5	0.309 (0.263)	0.17	177	transient hot-wire method	ref 14

to 0.55 W/(m K) (Figure 3a). As compared with the pure 1-octadecanol, the calculated TCE is 1.5 at 10 wt % pristine graphene content (Figure 3a). This enhancement can be attributed to the thermal conductive network of GSs fillers providing a pathway of lower resistance for phonon transport. The high aspect ratio and large interfacial contact area of GSs, as well as strong interface between GSs and the PCM matrix, may increase the thermal transport capacity of graphene-PCCs. However, the interface resistance, or so-called the Kapitza resistance, between organic molecules and GSs caused by the poor phonon coupling in the vibrational modes between PCM and GSs interfaces, decreases the overall thermal conductivity of the PCCs.[26] In addition, lattice defects induced by thermal exfoliation of the graphene oxides and the oxygen functional groups left on GSs because of the incompletely thermal reduction reduce the thermal conductivity of GSs significantly below the ideal value of defect-free graphene.[27,29,30]

As the interfacial resistance is inevitable upon the dispersion of fillers in the matrix and conjugated with a thick layer of 1-octadecanol, one feasible way to improve the thermal performance of PCCs is to use defect-free graphene with improved intrinsic thermal properties as fillers to form highly conductive networks for rapid heat transfer. Particularly, for carbonaceous materials, heat conduction is dominated by phonon transport from lattice vibrations of the covalent sp^2 bonding network.[27,29,30] High-temperature annealing heals defects in the lattice structure and removes oxygen functional groups, and thus reduces the number of effective phonon scattering centers (Figure 1 and Figure S1 in the Supporting Information). This can lead to drastic improvements of the thermal properties of GSs. The thermal conductivities and TCEs of PCCs with 5 wt % loading fraction of annealed GSs from different temperatures are shown in Figure 3b. The thermal conductivity increases from 0.7 to 1.32 W/(m K) with increase of the annealing temperature for GSs from 1600 to 2200 °C. Correspondingly, the TCE increases from 2.18 to 5, which is much higher than that of PGPCC (10 wt % loading fraction with the TCE of 0.6). The increase of thermal conductivity and TCE with annealing temperature is mainly due to the continuous removal of oxygen functional groups and lattice defects on GS. Further increasing in annealing temperature above 2200 °C for GSs does not improve the thermal properties of PCCs, as the structure optimization is completed at 2200 °C for defect-free and high quality GSs. The thermal conductivities and TCEs of PCCs with different mass loading fraction of defect-free GSs annealed at 2200 °C have been measured and a breakthrough enhancement in the thermal property of PCCs is achieved (Figure 3c). The thermal conductivity of the PCC increase to 0.32 W/(m K) at an annealed GSs loading fraction of 1 wt % and monotonically increases to 3.55 W/(m K) at the loading of 10 wt %. This represents an over 640% enhancement as compared to the PCCs with pristine GSs fillers at a comparable loading (10 wt %) and 15-fold enhancement as compared to pure 1-octadecanol (Figure 3b). The highest thermal properties ever reported so far for organic PCM composites (see Table 1) can be attributed to synergistic effects of removal of functional groups, elimination of defects on the annealed GSs, and improved crystallinity upon high thermal annealing at 2200 °C.

The phase change enthalpy is another critical factor to evaluate high performance PCCs that can be used as a measure of its thermal energy storage capacity. The heating and freezing curves obtained with DSC measurements of pure 1-octadecanol, PGPCC and AGPCC are presented in Figure 4. It can be seen that pure 1-octadecanol has two phase change peaks during crystallization due to the existence of a metastable intermediate solid phase. The first phase change peak occurs at 35.31 °C, corresponding to the metastable solid−solid phase transition of the 1-octadecanol. The second peak occurs at 55.21 °C, corresponding to the liquid−metastable solid phase change. However, during melting the solid - solid and metastable solid - liquid phase transitions occur very close to each other (within 1−2 °C). Therefore, only a single melting peak is visible. These peaks are matched with pure 1-octadecanol peaks in the previous report.[26,44] Identically, the PCCs show two crystallization temperatures (T_c) and single melting temperature (T_m) on DSC curves (Figure 4a, b).

In case of PGPCC, the T_c decreases and the T_m increases with increasing graphene content, and crystallization and melting became less exothermic/endothermic, respectively, in

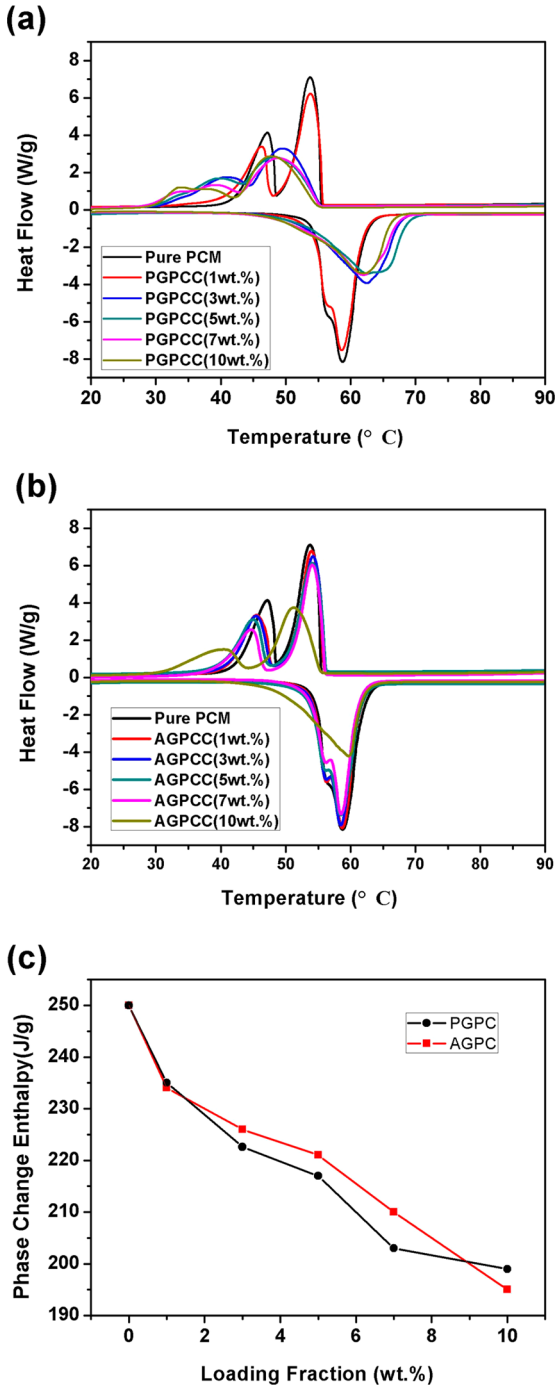

Figure 4. Differential scanning calorimetry (DSC) and phase change enthalpy of PCCs as a function of graphene loading: DSC plots of PCCs for (a) PGPCC and (b) AGPCC; and (c) phase change enthalpy of PCCs.

the presence of defective GSs.[26,45−47] The polar oxygen functional groups and large surface area of the 2D pristine GSs have a strong interaction with the matrix molecules, hindering the rearrangement and diffusion of molecular chains during crystallization and melting processes and enlarging the subcooling ($T_m - T_c$).[26,45−47] In contrast, the shift of crystallization temperatures of AGPCC is relatively small, and the melting temperature does not increase until up to 10 wt % GSs loading. The functional oxygen functional groups have been removed by high temperature annealing, weakening the interaction between annealed GSs and matrix. The hindering of crystallization and melting of AGPCC happens only at a large loading fraction of GSs (e.g., 10 wt %).[26,45−47] Unlike the pristine GSs, the less interaction between annealed graphene sheets and PCM molecules ensure that melting and solidification proceed in a narrow temperature range. Figure 4c shows that with the addition of GSs, the phase change enthalpy of 1-octadecanol decreases. At 5 wt % GSs loading, the phase change enthalpy shows a minor reduction to 222−225 J/g. The phase change enthalpies decrease to 79.6 and 78% in the case of 10 wt % pristine GSs and annealed GSs filler content. Nevertheless, the phase change enthalpies are still as high as 199 and 195 J/g for PGPCC and AGPCC at 10 wt % GSs loading, respectively. The decrease is expected given that some of the PCM volume is now replaced by the GSs that do not undergo phase change. We did not increase the GSs weight fraction beyond 10 wt % to avoid further reduction in the melting enthalpy.

Table 1 summarizes previously reported thermal conductivities and the calculated TCE values for PCC with various fillers. The comparison highlights that the measured TCE and thermal conductivity in the AGPCC are indeed extremely high. In previous reports on graphene-PCCs, PCCs at comparable graphene loading fractions delivered a much lower TCE (e.g., at 4−5 wt % loading fraction with a TCE of 1.39−2.96) because of the low-quality GSs with undesired functional groups and defects induced from the chemical synthesis and solution exfoliation processes.[11,14,20,26] Our AGPCC display a significantly enhanced TCE of 5 at a 5 wt % loading fraction. In case of annealed graphene aerogel, the 3D porous structure provided a compatible framework for filling with PCM.[12] However, the inadequate annealing process did not allow for a full recovery the graphene 's thermal properties. A higher filling fraction of ∼15 wt % loading fraction is required to achieve TCE 13.3,[12] still lower than AGPCC (10 wt % loading fraction with the TCE of 15.1). These results demonstrate that high temperature annealing can significantly improve the intrinsic thermal properties of chemically synthesized GSs and thus the composites with annealed graphene as nanofillers. Other carbon materials, such as graphite nanoplatelets, expanded graphite, carbon nanotubes and nanofibers have also been widely applied to improve the thermal conductivity of PCMs.[10,13,14,17,18,20] In the case of graphite nanoplatelets, loading fraction of 5−10 wt % leads to a TCE of 1.88−9.8.[18,20] Ten weight percent loading fraction of expanded graphite leads a even lower TCE of 2.73.[10] Carbon nanotubes and carbon nanofibers with a loading fraction of 5 wt % in PCM lead only to a minor increase in the TCE of 0.17−0.26 and 0.29−0.45, respectively,[13,14,17] whereas a comparable adding of ∼5−10 wt % annealed GSs into PCM lead to a much higher TCE up to 5−15.1, meanwhile maintaining a high phase-change enthalpy (∼200 J/g or above), indicating the superiority of annealed GSs as conductive nanofillers for organic PCMs as compared to other carbon forms.

3.3. Fast Transient Temperature Response and Effective Heat Transfer. The defect-free graphene/PCC shows immense potentials for advanced thermal energy storage and heat transfer materials due to their exceptional thermal conductivity. The transient temperature response behavior is compared among AGPCC (with 10 wt % loading fraction of 2200 °C annealed GSs), PGPCC (with 10 wt % loading fraction of pristine GSs) and pure 1-octadecanol. Samples were casted in disks and loaded into cylindrical molds to avoid

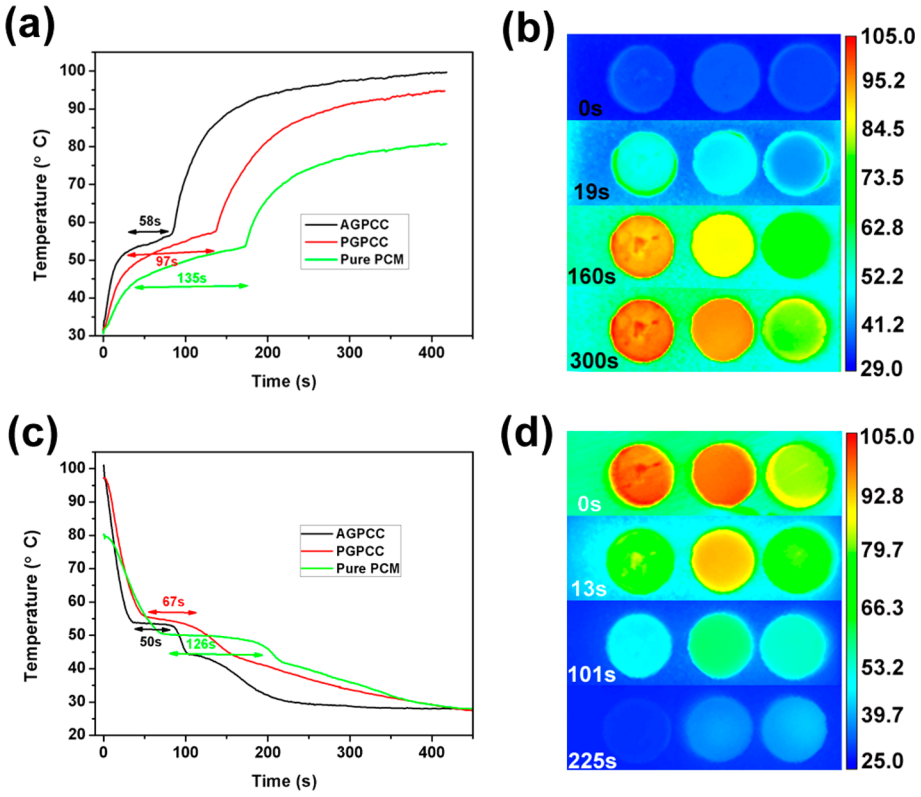

Figure 5. Rapid temperature response and effective heat transfer: (a) temperature response of PCCs during heating; (b) infrared camera images of PCCs at different heating times; (c) temperature response of PCCs during cooling; and (d) infrared camera images of PCCs at different cooling times. In the infrared images, the left sample is AGPCC, the middle sample is PGPCC, and the right sample is pure PCM. All of the samples have an identical thickness of 2 mm and diameter of 12.7 mm.

leakage during heating. An infrared camera was used to record the temperature response during heating and cooling. During heating, samples in molds were put on an isothermal hot plate with a constant temperature of 105 °C. As shown in Figure 5a, temperature increase is much faster in the AGPCC, indicating a higher rate of thermal diffusion, than PGPCC and pure 1-octadecanol. When approaching T_m, phase change occurs and the surface temperature of PCC remains stable as a flat plateau shown on heating curve during the phase transition from solid to liquid. The plateau length represents the time required to complete the phase change, which is much shorter for AGPCC (58 s) than those of PGPCC (97 s) and pure 1-octadecanol (135 s). The high thermal conductivity provides a fast heat transfer rate, enabling AGPCC to absorb thermal energy more rapidly during phase change. After phase change, the PCCs were heated continuously until steady state approached. The final surface temperature of defect-free graphene/PCC is 101 °C, which is higher than that of PGPCC (94 °C) and pure 1-octadecanol (80 °C). The high-quality annealed GSs with complete removal of defects and functional groups induce a lower thermal resistance for the AGPCC upon the uniform distribution of highly thermally conductive fillers so that the temperature gradient inside of AGPCC is smaller than that of PGPCC and pure 1-octadecanol. Temperature rise can also be directly seen in infrared camera images represented by the color change from blue to red in Figure 5b. At the initial state, three samples show a uniform blue color. As time increases, the color of three samples shows a drastic difference. The surface temperature of the AGPCC is always higher than others at different durations, e.g., at t = 19 s, t = 160 s, and the steady state (t = 300 s). Because of the high thermal conductivity contributed by defect-free GSs, AGPCC shows a high thermal energy absorbing rate during phase transition, highlighting its potential to be used as cooling material to mitigate overheating of electronics at the peak power and also a more effective storage of solar energy when working as phase change materials for latent energy storage.

After steady state, the PCCs were transferred to a stainless steel plate to cool down. The cooling curves were recorded as shown in Figure 5c. At the beginning, the temperature of the AGPCC (101 °C) was higher than that of PGPCC (97 °C) and pure PCM (80 °C), attributed to the higher steady-state temperature during heating due to the high thermal conductivity. As time increased, the rate of temperature drop in the AGPCC was much higher than the PGPCC and pure PCM (Figure 5c). When T_c approached, temperature plateaus show on the cooling curves, representing the phase transition from liquid to solid. The plateau length is much shorter for AGPCC (50 s) than that of PGPCC (67 s) and pure 1-octadecanol (126 s), indicating AGPCC can release the stored thermal energy at a higher rate during phase change. The temperature drop can also be directly seen from the infrared camera images during cooling (Figure 5d). Initially, a large (~20 °C) temperature difference exists between AGPCC and pure PCM, represented by the dramatic color difference on the infrared camera image (Figure 5d, t = 0). After a short time interval, the surface temperature of AGPCC approaches to that of pure PCM at a high cooling rate (Figure 5d, t = 13 s). With increased time, the surface temperature of the AGPCC continuously decreases at high rate and remains lower than

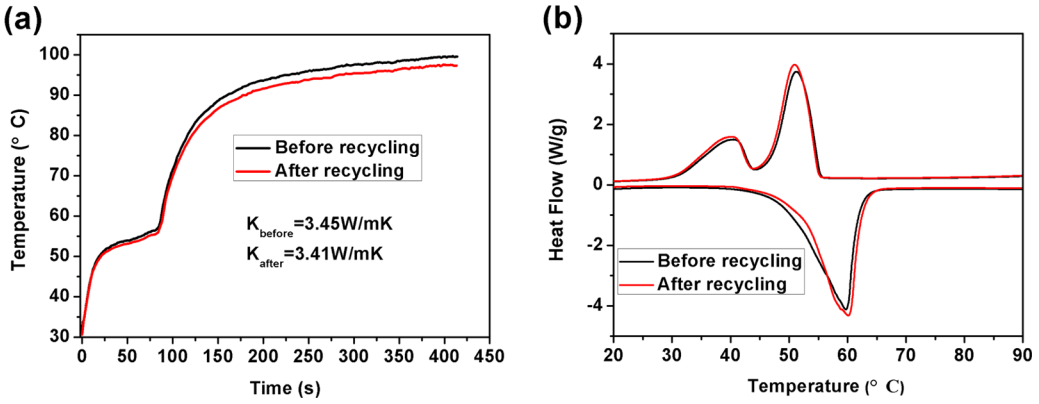

Figure 6. (a) Transient temperature response of PCC before and after recycling; (b) DSC plots for PCC before and after recycling.

these of the PGPCC and pure PCM, as shown when t = 101 and 225 s. The faster cooling rate is essential for the AGPCCs to release stored thermal energy at a rate high enough for effective thermal management.

3.4. Thermal Recycling Stability. For practical applications, thermal properties of PCCs must be stable after multiple melting and solidification cycles. To evaluate the thermal recycling stability of the composites, transient temperature responses have been compared for the AGPCC sample (with 10 wt % loading fraction of 2200 °C annealed GSs) before and after melting-solidification cycles. PCC was melt at 105 °C on a hot plate and then solidified at 20 °C repeatedly for 50 cycles. Sample was casted in disk and heated on the isothermal hot plate with a constant temperature of 105 °C. The temperature response curves (Figure 6a) recorded by thermal infrared camera are virtually identical for the sample before and after recycling. The thermal conductivity has also been checked, showing a very minor change (less than 2%) for the sample before and after melting-solidification cycles. Additionally, the PCC was then checked with DSC for the latent heat storage capacity (Figure 6b). Compared with 195 J/g for the original sample, the latent heat of sample was 198 J/g after 50 melting-solidification cycles. The measurement of transient temperature response, thermal conductivity and phase change enthalpy show excellent thermal reversibility of the PCC, even after operating for 50 cycles. The high thermal stability can be attributed to the compatible interface between the GSs and 1-octadecanol and the uniform distribution of GSs in PCM, preventing the agglomeration of graphene during the phase transition from solid to liquid.

4. CONCLUSIONS

In conclusion, defect-free graphene sheets are obtained through high-temperature thermal annealing to eliminate defects and oxygen functional groups. Used as nanoscale fills, the defect-free GSs can greatly improve the thermal conductivity of the organic phase change composite because of the elimination of effective phonon scattering centers for thermal transport with only a small reduction in the heat of fusion. A high thermal conductivity of 3.55 W/(m K) has been achieved for defect-free graphene/PCCs at a 10 wt % loading, and the phase change enthalpy maintains at ~200 J/g. This represents an over 600% enhancement as compared to the PCCs with pristine GSs fillers at a comparable loading (10 wt %) and 15-fold enhancement as compared to pure 1-octadecanol. The breakthrough enhancement for defect-free graphene PCCs is superior to the state-of-the-art of phase change composites with defect graphenes, graphite nanoplatelets or graphene aerogels, carbon nanotubes, and carbon nanofibers as fillers in literatures. The highest thermal conductivity ever reported, rapid temperature response, effective heat transfer efficiency, and high thermal stability highlight the immense potential of the defect-free graphene/organic phase change composites for superior thermal management and advanced thermal energy storage systems with transformational performance.

■ ASSOCIATED CONTENT

Supporting Information

Deconvoluted C1s spectra. This material is available free of charge via the Internet at http://pubs.acs.org.

■ AUTHOR INFORMATION

Corresponding Authors

*E-mail: gran@xmu.edu.cn.
*E-mail: lianj@rpi.edu.

Notes

The authors declare no competing financial interest.

■ ACKNOWLEDGMENTS

This work is financially supported by a NSF Career Award DMR 1151028.

■ REFERENCES

(1) Mondal, S. Phase Change Materials for Smart Textiles – An Overview. *Appl. Therm. Eng.* **2008**, *28*, 1536–1550.
(2) Sharma, A.; Tyagi, V. V.; Chen, C. R.; Buddhi, D. Review on Thermal Energy Storage with Phase Change Materials and Applications. *Renewable Sustainable Energy Rev.* **2009**, *13*, 318–345.
(3) Fan, L.; Khodadadi, J. M. Thermal Conductivity Enhancement of Phase Change Materials for Thermal Energy Storage: A Review. *Renewable Sustainable Energy Rev.* **2011**, *15*, 24–46.
(4) Nabil, M.; Khodadadi, J. M. Experimental Determination of Temperature-Dependent Thermal Conductivity of Solid Eicosane-Based Nanostructure-Enhanced Phase Change Materials. *Int. J. Heat Mass Transfer* **2013**, *67*, 301–310.
(5) Khodadadi, J. M.; Fan, L.; Babaei, H. Thermal Conductivity Enhancement of Nanostructure-Based Colloidal Suspensions Utilized as Phase Change Materials for Thermal Energy Storage: A Review. *Renewable Sustainable Energy Rev.* **2013**, *24*, 418–444.
(6) Mesalhy, O.; Lafdi, K.; Elgafy, A. Carbon Foam Matrices Saturated with PCM for Thermal Protection Purposes. *Carbon* **2006**, *44*, 2080–2088.
(7) Chintakrinda, K.; Weinstein, R. D.; Fleischer, A. S. A Direct Comparison of Three Different Material Enhancement Methods on

the Transient Thermal Response of Paraffin Phase Change Material Exposed to High Heat Fluxes. *Int. J. Therm. Sci.* **2011**, *50*, 1639−1647.
(8) Pincemin, S.; Christ, M.; Oettinger, O.; Py, X.; Olives, R. Elaboration of Conductive Thermal Storage Composites Made of Phase Change Materials and Graphite for Solar Plant. *J. Sol. Energy Eng.* **2007**, *130*, 011005−011005.
(9) Lafdi, K.; Elgafy, A.; Mesalhy, O. Merits of Employing Foam Encapsulated Phase Change Materials for Pulsed Power Electronics Cooling Applications. *J. Electron. Packag.* **2008**, *130*, 021004−021004.
(10) Sarı, A.; Karaipekli, A. Thermal Conductivity and Latent Heat Thermal Energy Storage Characteristics of Paraffin/Expanded Graphite Composite as Phase Change Material. *Appl. Therm. Eng.* **2007**, *27*, 1271−1277.
(11) Li, H.; Jiang, M.; Li, Q.; Li, D.; Chen, Z.; Hu, W.; Huang, J.; Xu, X.; Dong, L.; Xie, H.; Xiong, C. Aqueous Preparation of Polyethylene Glycol/Sulfonated Graphene Phase Change Composite with Enhanced Thermal Performance. *Energy Convers. Manage.* **2013**, *75*, 482−487.
(12) Zhong, Y.; Zhou, M.; Huang, F.; Lin, T.; Wan, D. Effect of Graphene Aerogel on Thermal Behavior of Phase Change Materials for Thermal Management. *Sol. Energy Mater. Sol. Cells* **2013**, *113*, 195−200.
(13) Zeng, J. L.; Cao, Z.; Yang, D. W.; Xu, F.; Sun, L. X.; Zhang, X. F.; Zhang, L. Effects of MWNTs on Phase Change Enthalpy and Thermal Conductivity of A Solid-Liquid Organic PCM. *J. Therm. Anal. Calorim.* **2009**, *95*, 507−512.
(14) Fan, L.-W.; Fang, X.; Wang, X.; Zeng, Y.; Xiao, Y.-Q.; Yu, Z.-T.; Xu, X.; Hu, Y.-C.; Cen, K.-F. Effects of Various Carbon Nanofillers on the Thermal Conductivity and Energy Storage Properties of Paraffin-Based Nanocomposite Phase Change Materials. *Appl. Energy* **2013**, *110*, 163−172.
(15) Sanusi, O.; Warzoha, R.; Fleischer, A. S. Energy Storage and Solidification of Paraffin Phase Change Material Embedded with Graphite Nanofibers. *Int. J. Heat Mass Transfer* **2011**, *54*, 4429−4436.
(16) Ji, H.; Sellan, D. P.; Pettes, M. T.; Kong, X.; Ji, J.; Shi, L.; Ruoff, R. S. Enhanced Thermal Conductivity of Phase Change Materials with Ultrathin-Graphite Foams for Thermal Energy Storage. *Energy Environ. Sci.* **2014**, *7*, 1185.
(17) Cui, Y.; Liu, C.; Hu, S.; Yu, X. The Experimental Exploration of Carbon Nanofiber and Carbon Nanotube Additives on Thermal Behavior of Phase Change Materials. *Sol. Energy Mater. Sol. Cells* **2011**, *95*, 1208−1212.
(18) Kim, S.; Drzal, L. T. High Latent Heat Storage and High Thermal Conductive Phase Change Materials Using Exfoliated Graphite Nanoplatelets. *Sol. Energy Mater. Sol. Cells* **2009**, *93*, 136−142.
(19) Zhou, M.; Lin, T.; Huang, F.; Zhong, Y.; Wang, Z.; Tang, Y.; Bi, H.; Wan, D.; Lin, J. Highly Conductive Porous Graphene/Ceramic Composites for Heat Transfer and Thermal Energy Storage. *Adv. Funct. Mater.* **2013**, *23*, 2263−2269.
(20) Shi, J.-N.; Ger, M.-D.; Liu, Y.-M.; Fan, Y.-C.; Wen, N.-T.; Lin, C.-K.; Pu, N.-W. Improving the Thermal Conductivity and Shape-Stabilization of Phase Change Materials Using Nanographite Additives. *Carbon* **2013**, *51*, 365−372.
(21) Yu, Z.-T.; Fang, X.; Fan, L.-W.; Wang, X.; Xiao, Y.-Q.; Zeng, Y.; Xu, X.; Hu, Y.-C.; Cen, K.-F. Increased Thermal Conductivity of Liquid Paraffin-Based Suspensions in the Presence of Carbon Nano-Additives of Various Sizes and Shapes. *Carbon* **2013**, *53*, 277−285.
(22) Xiang, J.; Drzal, L. T. Investigation of Exfoliated Graphite Nanoplatelets (XGnP) in Improving Thermal Conductivity of Paraffin Wax-Based Phase Change Material. *Sol. Energy Mater. Sol. Cells* **2011**, *95*, 1811−1818.
(23) Zhao, J.; Guo, Y.; Feng, F.; Tong, Q.; Qv, W.; Wang, H. Microstructure and Thermal Properties of A Paraffin/Expanded Graphite Phase-Change Composite for Thermal Storage. *Renewable Energy* **2011**, *36*, 1339−1342.
(24) Li, M. A Nano-Graphite/Paraffin Phase Change Material with High Thermal Conductivity. *Appl. Energy* **2013**, *106*, 25−30.
(25) Hosseinizadeh, S. F.; Darzi, A. A. R.; Tan, F. L. Numerical Investigations of Unconstrained Melting of Nano-Enhanced Phase Change Material (NEPCM) Inside a Spherical Container. *Int. J. Therm. Sci.* **2012**, *51*, 77−83.
(26) Yavari, F.; Fard, H. R.; Pashayi, K.; Rafiee, M. A.; Zamiri, A.; Yu, Z.; Ozisik, R.; Borca-Tasciuc, T.; Koratkar, N. Enhanced Thermal Conductivity in A Nanostructured Phase Change Composite due to Low Concentration Graphene Additives. *J. Phys. Chem. C* **2011**, *115*, 8753−8758.
(27) Ghosh, S.; Bao, W.; Nika, D. L.; Subrina, S.; Pokatilov, E. P.; Lau, C. N.; Balandin, A. A. Dimensional Crossover of Thermal Transport in Few-Layer Graphene. *Nat. Mater.* **2010**, *9*, 555−558.
(28) Xin, G.; Hwang, W.; Kim, N.; Cho, S. M.; Chae, H. A Graphene Sheet Exfoliated with Microwave Irradiation and Interlinked by Carbon Nanotubes for High-Performance Transparent Flexible Electrodes. *Nanotechnology* **2010**, *21*, 405201.
(29) Balandin, A. A.; Ghosh, S.; Bao, W.; Calizo, I.; Teweldebrhan, D.; Miao, F.; Lau, C. N. Superior Thermal Conductivity of Single-Layer Graphene. *Nano Lett.* **2008**, *8*, 902−907.
(30) Balandin, A. A. Thermal Properties of Graphene and Nanostructured Carbon Materials. *Nat. Mater.* **2011**, *10*, 569−581.
(31) Zhu, Y.; Murali, S.; Cai, W.; Li, X.; Suk, J. W.; Potts, J. R.; Ruoff, R. S. Graphene and Graphene Oxide: Synthesis, Properties, and Applications. *Adv. Mater.* **2010**, *22*, 3906−3924.
(32) Chen, D.; Feng, H.; Li, J. Graphene Oxide: Preparation, Functionalization, and Electrochemical Applications. *Chem. Rev.* **2012**, *112*, 6027−6053.
(33) Hernandez, Y.; Nicolosi, V.; Lotya, M.; Blighe, F. M.; Sun, Z.; De, S.; McGovern, I. T.; Holland, B.; Byrne, M.; Gun'Ko, Y. K.; Boland, J. J.; Niraj, P.; Duesberg, G.; Krishnamurthy, S.; Goodhue, R.; Hutchison, J.; Scardaci, V.; Ferrari, A. C.; Coleman, J. N. High-Yield Production of Graphene by Liquid-Phase Exfoliation of Graphite. *Nat. Nanotechnol.* **2008**, *3*, 563−568.
(34) Xin, G.; Gong, S.; Kim, N.; Kim, J.; Hwang, W.; Nam, J.; Cho, Y.-H.; Cho, S. M.; Chae, H. Graphene Oxide/N-methyl-2-pyrrolidone Charge-Transfer Complexes for Molecular Detection. *Sens. Actuators, B* **2013**, *176*, 81−85.
(35) Xin, G.; Wang, H.; Kim, N.; Hwang, W.; Cho, S. M.; Chae, H. Investigation of Charge-Transfer Complexes Formation between Photoluminescent Graphene Oxide and Organic Molecules. *Nanoscale* **2012**, *4*, 405−407.
(36) Xin, G.; Meng, Y.; Ma, Y.; Ho, D.; Kim, N.; Cho, S. M.; Chae, H. Tunable Photoluminescence of Graphene Oxide from Near-Ultraviolet to Blue. *Mater. Lett.* **2012**, *74*, 71−73.
(37) Yu, J.; Qian, R.; Jiang, P. Enhanced Thermal Conductivity for PVDF Composites with A Hybrid Functionalized Graphene Sheet-Nanodiamond Filler. *Fibers Polym.* **2013**, *14*, 1317−1323.
(38) Shahil, K. M. F.; Balandin, A. A. Graphene−Multilayer Graphene Nanocomposites as Highly Efficient Thermal Interface Materials. *Nano Lett.* **2012**, *12*, 861−867.
(39) Song, W.-L.; Wang, W.; Veca, L. M.; Kong, C. Y.; Cao, M.-S.; Wang, P.; Meziani, M. J.; Qian, H.; LeCroy, G. E.; Cao, L.; Sun, Y.-P. Polymer/Carbon Nanocomposites for Enhanced Thermal Transport Properties - Carbon Nanotubes Versus Graphene Sheets as Nanoscale Fillers. *J. Mater. Chem.* **2012**, *22*, 17133−17139.
(40) Song, L.; Khoerunnisa, F.; Gao, W.; Dou, W.; Hayashi, T.; Kaneko, K.; Endo, M.; Ajayan, P. M. Effect of High-Temperature Thermal Treatment on the Structure and Adsorption Properties of Reduced Graphene Oxide. *Carbon* **2013**, *52*, 608−612.
(41) Jin, M.; Kim, T. H.; Lim, S. C.; Duong, D. L.; Shin, H. J.; Jo, Y. W.; Jeong, H. K.; Chang, J.; Xie, S.; Lee, Y. H. Facile Physical Route to Highly Crystalline Graphene. *Adv. Funct. Mater.* **2011**, *21*, 3496−3501.
(42) Zhang, Y.; Li, D.; Tan, X.; Zhang, B.; Ruan, X.; Liu, H.; Pan, C.; Liao, L.; Zhai, T.; Bando, Y.; Chen, S.; Cai, W.; Ruoff, R. S. High Quality Graphene Sheets from Graphene Oxide by Hot-Pressing. *Carbon* **2013**, *54*, 143−148.
(43) Ohki, K.; Kowalczyk, L. S. Thermal Conductivity of Some Organic Compounds at Their Melting Points. *J. Chem. Eng. Data* **1964**, *9*, 220−221.

(44) Ventolà, L.; Ramírez, M.; Calvet, T.; Solans, X.; Cuevas-Diarte, M. A.; Negrier, P.; Mondieig, D.; van Miltenburg, J. C.; Oonk, H. A. J. Polymorphism of N-Alkanols: 1-Heptadecanol, 1-Octadecanol, 1-Nonadecanol, and 1-Eicosanol. *Chem. Mater.* **2002**, *14*, 508−517.
(45) Lai, M.; Kim, J.-K. Effects of Epoxy Treatment of Organoclay on Structure, Thermo-Mechanical and Transport Properties of Poly-(ethylene terephthalate-co-ethylene naphthalate)/Organoclay Nanocomposites. *Polymer* **2005**, *46*, 4722−4734.
(46) Raghu, A. V.; Lee, Y. R.; Jeong, H. M.; Shin, C. M. Preparation and Physical Properties of Waterborne Polyurethane/Functionalized Graphene Sheet Nanocomposites. *Macromol. Chem. Phys.* **2008**, *209*, 2487−2493.
(47) Jeong, H.; Kim, B.; Kim, E. Structure and Properties of EVOH/Organoclay Nanocomposites. *J. Mater. Sci.* **2005**, *40*, 3783−3787.